ACS Sustainable Chemistry & Engineering

Research Article

Cite This: ACS Sustainable Chem. Eng. 2019, 7, 12897−12909

pubs.acs.org/journal/ascecg

Sulfur-Mediated Mechanochemical Synthesis of Spherical and Needle-Like Copper Sulfide Nanocrystals with Antibacterial Activity

Zh. Shalabayev,*[,†] M. Baláž,[‡] N. Daneu,[§] E. Dutková,[‡] Z. Bujňáková,[‡] M. Kaňuchová,[∥] Z. Danková,[‡] Ľ. Balážová,[⊥] F. Urakaev,[#] Ľ. Tkáčiková,[⊥] and M. Burkitbayev[†]

[†]Al-Farabi Kazakh National University, Al-Farabi ave., 71, 050040 Almaty, Kazakhstan

[‡]Institute of Geotechnics, Slovak Academy of Sciences, Watsonova 45, 04001 Košice, Slovakia

[§]Jožef Stefan Institute, Jamova cesta 39, 1000 Ljubljana, Slovenia

[∥]Faculty of Mining, Ecology, Process Control and Geotechnologies, Technical University, Letná 9 04200 Košice, Slovakia

[⊥]University of Veterinary Medicine and Pharmacy, Komenského 73, 04181 Košice, Slovakia

[#]Sobolev Institute of Geology and Mineralogy SB RAS, Academic Koptyug str. 3, 630090 Novosibirsk, Russia

Supporting Information

ABSTRACT: In the present study, a quick and environmentally friendly approach has been developed for the synthesis of CuS nanocrystals of different shape with antibacterial activity. The process is completed in 5 min. The presence of copper sulfide in the final products was confirmed by XRD, Raman spectroscopy, XPS, and TEM. The morphology of the product is dependent on whether or not the reaction providing sulfur was realized. When sulfur was included, the CuS particles developed an elongated shape with a thickness in the range between 6 and 8 nm and lengths up to 60 nm. It was found that sulfur plays a role of a nucleation agent in this case and then is removed during the washing process. On the other hand, if just precursors for copper sulfide were used, the morphology was spherical and the crystallite size was around 20 nm. Finally, the antibacterial activity of the products was evaluated. The activity was less selective in the case of CuS prepared by the assistance of sulfur.

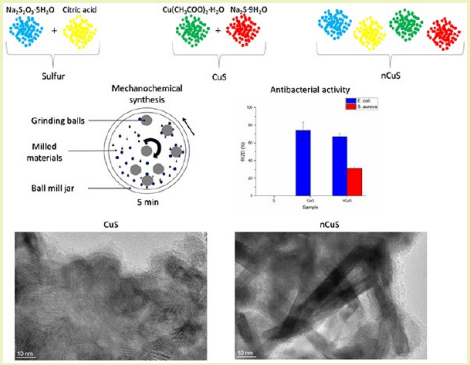

KEYWORDS: *mechanochemical synthesis, shape, copper sulfide, sulfur, nanocrystals, antibacterial activity*

INTRODUCTION

Semiconductor nanoparticles are used for various purposes (e.g., in solar cells, cathode material in lithium batteries, optical filters, or in photocatalysis).[1,2] Recently, physicochemical properties and application fields of copper sulfide semiconductors such as chalcocite (Cu_2S),[3,4] covellite (CuS),[5−7] villamaninite (CuS_2),[8] and nonstoichiometric copper sulfides (yarrowite ($Cu_{1.12}S$), anilite ($Cu_{1.75}S$), etc.)[9−11] are intensively studied. Among them, covellite (CuS) nanoparticles have an inevitable place, as they are promising materials for electrical, optical, environmental, as well as for biomedical applications.[12−16] There are also few studies reporting the antibacterial activity of CuS.[17−20] The utilization of copper-based nanoparticles as antimicrobial agents is a hot topic nowadays.[21−23]

There are many preparation methods of copper sulfide nanoparticles such as hydrothermal,[24] sonochemical,[25] microwave irradiation,[26] molecular template,[27] polyol,[28] chemical vapor deposition,[29] and mechanochemical synthesis.[30−32]

The last one is of particular interest as it utilizes a combination of the solid-state approach and mechanical energy for various purposes in an environmentally friendly way.[33] It can be applied in different research fields such as inorganic chemistry,[34] organic chemistry,[35] catalysis,[36] polymers,[37] cocrystals formation,[38] and waste management.[39] Since the mechanochemical approach reduces the use of harmful organic solvents and saves energy (no need of manual temperature increase), it is an environmentally method. Application fields of mechanochemistry are well described in the work of Boldyreva et al.[40]

As already mentioned, this method has been successfully applied for the production of CuS nanoparticles. Acetate route synthesis of MS (M: Zn, Cd, and Pb) nanoparticles utilizing mechanochemistry has been proposed by Baláž et al.[41] and using this approach Godočíková et al. synthesized copper sulfide nanoparticles in an industrial mill.[42]

Shape-controlled synthesis of CuS utilizing various solution-based methods was reported in the past. Reports showing the successful formation of various morphologies of CuS, such as a flower- and trepang-like,[43] pillar- and raft-like,[44] rod- and flake-like,[45] sphere-, urchin-, and tube-like[46,47] were published. However, no report of shape control using mechanochemistry was published until now.

Received: April 2, 2019
Revised: June 13, 2019
Published: July 9, 2019

DOI: 10.1021/acssuschemeng.9b01849
ACS Sustainable Chem. Eng. 2019, 7, 12897−12909

In this study, we have synthesized CuS nanocrystals via a simple and cost-efficient mechanochemical method. By introducing sulfur as a reaction intermediate on the pathway to the final product, the possibility to prepare nanoparticles in different shape was discovered. To our best knowledge, this is the first report on the mechanochemical synthesis of CuS with different shapes.

MATERIALS AND METHODS

Chemicals. Sodium thiosulfate ($Na_2S_2O_3 \cdot 5H_2O$, ITES, Slovakia), citric acid ($C_6H_8O_7$, Liana, Slovakia), copper acetate ($Cu(CH_3COO)_2 \cdot H_2O$, Acros Organics, Belgium), and sodium sulfide ($Na_2S \cdot 9H_2O$, Acros Organics, Belgium) were analytical grade and were used without further purification. Distilled water was used in all washing and cleaning procedures.

Mechanochemical Synthesis of S, CuS, and nCuS. For all milling experiments, the reactants (5 g) in stoichiometric amounts were transferred into a 250 mL steel milling chamber containing 50 steel balls with 10 mm diameter and milled for 1−15 min using the Pulverisette 6 planetary ball mill (Fritsch, Germany) using rotational speed 550 rpm, ball-to-powder ratio 37 and air atmosphere. After milling, the obtained product was washed with 1.5 L of water in order to remove the undesirable side-products and dried at 70 °C.

Sulfur particles were mechanochemically synthesized by the reaction of sodium thiosulfate pentahydrate with citric acid, thus mirroring the procedure reported in ref 48, according to the following reaction:

$$Na_2S_2O_3 \cdot 5H_2O + C_6H_8O_7(\text{catalyst}) \rightarrow S + Na_2SO_3 + C_6H_8O_7(\text{catalyst}) + 5H_2O \quad (1)$$

Citric acid has been used as a catalyst. In a typical procedure, 2.8133 g of sodium thiosulfate and 2.1817 g of citric acid was homogenized and milled.

Copper sulfide nanocrystals were prepared by the so-called acetate route following the procedure in ref 41 In this synthesis, copper acetate monohydrate and sodium sulfide nonahydrate were comilled in a stoichiometric amount (2.2727 and 2.7273 g, respectively), according to the chemical reaction:

$$Cu(CH_3COO)_2 \cdot H_2O + Na_2S \cdot 9H_2O \rightarrow CuS + 2CH_3COONa + 10H_2O \quad (2)$$

In order to obtain nCuS, the reactions 1 and 2 were realized simultaneously.

Characterization Methods and Techniques. The XRD patterns were recorded by a D8 Advance diffractometer (Bruker, Germany) with CuKα (40 kV, 40 mA) radiation. XRD patterns were measured in the 2 theta range 10−60° with step size 0.03° and step time 6 s. For phase analysis, the JCPDS-PDF2 database and the Diffrac^{plus} EVA software has been used.

The Raman data were obtained using a combined system Solver Spectrum (NT-MDT Spectrum Instruments, Russia), equipped with a photomultiplier tube (PMT) detector, a high-stability fast confocal laser (Rayleigh) imaging and 600/600 grating, 473 nm solid state laser excitation. In all experiments, laser power at the sample was 35 mW and the exposure time was 60 s. Continuously tunable filters ND = 0.5 which reduce the laser intensity by 30% were also used. Without the use of a filter, the sulfur sample is decomposed by the laser action. When using a blue laser, an error of ±4 cm^{-1} is provided.

The absorption spectra were measured using a UV−vis spectrophotometer Helios Gamma (Thermo Electron Corporation, Great Britain) in the range of 300−900 nm using a 1 cm path length quartz cuvette. The samples were diluted in absolute ethanol by ultrasonic stirring.

The PL spectra at room temperature were recorded at right angle on a photon counting spectrofluorometer PC1 (ISS, USA) with an excitation wavelength of 350 nm. A 300 W xenon lamp was used as the excitation source. Excitation and emission slit widths were set to 1 and 2 mm, respectively. One cm path length rectangular quartz cuvette was used. The PL intensity was measured from the powder samples ultrasonically dispersed in absolute ethanol.

The surfaces of samples were analyzed by X-ray photoelectron spectroscopy (XPS). XPS measurements were performed using XPS instrument (SPECS) equipped with PHOIBOS 100 SCD and nonmonochromatic X-ray source. The survey surface spectrum was measured at 70 eV transition energy and core spectra at 20 eV at room temperature. All spectra were acquired at a basic pressure of 9×10^{-9} mbar with AlK_α excitation at 200 W. The data were analyzed by SpecsLab2 CasaXPS software (Casa Software Ltd.). A Shirley and Tougaard type baseline was used for all peak-fits. The spectrometer was calibrated against silver (Ag 3d). All samples showed variable degrees of charging due to their insulating nature. The problem was resolved by the calibration on carbon.

The particle size distribution was measured by photon cross-correlation spectroscopy (PCCS) using a particle size analyzer Nanophox (Sympatec, Germany). The powdered samples were dispersed in distilled water and sonicated before measurements. A portion of each sample was subsequently diluted with distilled water to achieve a suitable concentration for measurement. This analysis was performed using a dispersant refractive index of 1.33. The measurements were repeated 3 times for each sample.

Scanning electron microscopic (SEM) analysis of the samples was carried out with a SEM Quanta 3D 200i instrument (FEI, The Netherlands). Conducting carbon adhesive tape was used as a substrate for the samples. SEM images of the not washed and dried filtrate samples of nCuS system were recorded using a MIRA3 FE-SEM microscope (TESCAN, Czech Republic) equipped with EDX detector (Oxford Instrument, United Kingdom). Nanoscale analyses of the samples were performed by transmission electron microscopy (TEM). For TEM analyses, the samples were ultrasonically dispersed in absolute ethanol and the fine fraction of each sample was carefully applied onto a carbon-coated nickel grid. The dried grids were additionally carbon coated to prevent charging under the high-energy electron beam. TEM analyses were performed using a 200 kV microscope JEM 2100 (JEOL, Japan) with LaB_6 electron source.

Antibacterial Activity. The antibacterial activity of the samples was evaluated by the agar well diffusion method by a slight modification of the process reported in.[49] The tested bacteria (*S. aureus* CCM 4223, and *E. coli* CCM 3988) were obtained from the Czech collection of microorganisms (CCM).

In brief, bacteria were cultured aerobically at 37 °C in nutrient broth (Oxoid, United Kingdom) with agitation, or on standard plate count agar (Oxoid, United Kingdom). Frozen stock cultures were maintained at −20 °C. Before the experimental use, cultures were transferred to liquid media and incubated for 24 h. Cultures were then subcultured in liquid media, incubated for 24 h and used as the source of inoculum for each experiment.

Agar media was cooled to 42 °C after autoclaving, inoculated with liquid overnight bacterial culture to a cell density of 5×10^5 cfu/mL and 20 mL of this inoculated agar was pipetted into a 90 mm diameter Petri dish. Prior to the measurement, 10 mg of each sample was dispersed in 1 mL distilled water using sonication. After the solidification of agar, five millimeters diameter wells were punched into it and filled with 50 μL of samples. Distilled water was used as negative control and gentamicin sulfate (Sigma-Aldrich, U.S.A.) with the concentration 10 mM as a positive control. The plates were incubated for 24 h at 37 °C. After the incubation, the plates were photographed and the inhibition zones were measured by the ImageJ software. The values used for the calculation were the mean values of three replicate tests. The antibacterial activity was calculated by applying the formula:

$$\%RIZD = [(IZD\ \text{sample} - IZD\ \text{negative control}) / IZD\ \text{gentamicin}] \times 100 \quad (3)$$

where RIZD is the percentage of relative inhibition zone diameter and IZD is the inhibition zone diameter (mm). As a negative control, the inhibition zones of distilled water equal to 0 were taken. The inhibition zone diameter (IZD) was obtained by measuring the diameter of the transparent zone and subtracting the size of the wells (5 mm).

DOI: 10.1021/acssuschemeng.9b01849
ACS Sustainable Chem. Eng. 2019, 7, 12897−12909

RESULTS AND DISCUSSION

XRD Analyses. As a first step, it was necessary to prepare sulfur particles. In Figure 1, the X-ray diffraction patterns of

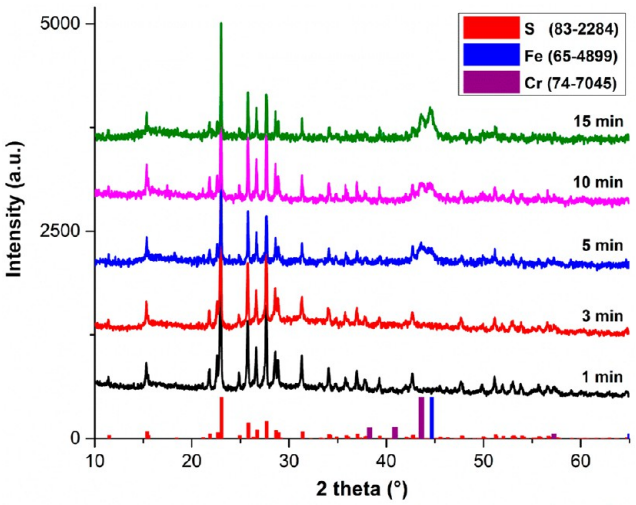

Figure 1. XRD patterns of sulfur prepared by milling of STS and CA for a different time.

sodium thiosulfate pentahydrate (STS) milled for 1, 3, 5, 10, and 15 min in the presence of citric acid (CA) are shown. The patterns were recorded after the washing procedure. The XRD patterns prior to washing procedure showing sulfur and unidentified reflections are provided in the ESI (Figure S1).

It can be clearly seen that almost all diffraction peaks of the washed samples can be surely ascribed to sulfur and there seems to be no difference with respect to milling time. However, in addition to sulfur peaks, there are some diffuse peaks present around 45° for the samples milled for more than 5 min. These two peaks at 43.6° and 44.7° can be ascribed to chromium and iron respectively and are a result of contamination from the milling chamber. Their intensity increases with prolonged milling. It seems that this reaction causes a significant amount of chromium and iron from milling media to enter the reaction mixture after a very short time. The intensity of these peaks increases with milling time, which supports the hypothesis about wear.[50]

Using a similar approach, Urakaev et al. synthesized sulfur nanoparticles via the reaction of sodium thiosulfate pentahydrate with crystalline succinic acid ($C_4H_6O_4$).[48] In their work, the concept of the diluent agent (side final product, Na_2SO_3) was used. The main idea of this approach is a dilution of the initial reaction system by a compound, which will not react with reagents and products, and thus dilutes the product to form smaller nanocrystallites.[51,52]

In our case, the dilution strategy was not applied, however, in comparison with Urakaev et al.,[48] the synthesis time was significantly reduced. As the diffraction peaks seem to be very sharp in our case, the size of crystallites is most probably in the micrometer range.

Subsequently, the synthesis of copper sulfide using the acetate route was realized. Figure 2 shows the XRD patterns of the washed powders after milling copper acetate and sodium sulfide for different times. The XRD patterns prior to washing procedure showing CuS and most probably hydrated forms of copper sulfates are provided in the ESI (Figure S2). The diffraction peaks in the patterns of the washed samples closely

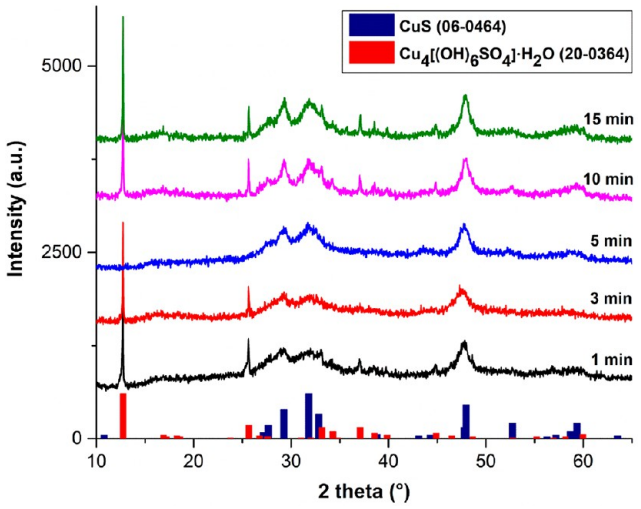

Figure 2. XRD patterns of copper sulfide prepared by milling of copper acetate and sodium sulfide for a different time.

match those of copper sulfide from the database (JCPDS 06-0464). As shown in the XRD pattern (Figure 2), only 5 min of milling are satisfactory for the reaction, as no other peaks were detected, indicating the high purity of the sample. All the other samples contain posnjakite phase ($Cu_4[(OH)_6SO_4]\cdot H_2O$; JCPDS 20-0364). We are unable to explain this phenomenon at the moment, but it was observed also upon repeated experiment. The presence of hydrated copper sulfates (namely chalcanthite and bonattite phases) was also detected upon the semi-industrial mechanochemical synthesis of CuS using this approach before.[42] From the XRD pattern (Figure 2) it seems that the crystallite size most probably increases with milling time (as documented by increase in the intensity of diffraction peaks).

The above-mentioned facts suggest that for both S and CuS formation, 5 min of milling seem to be the best option. Both reactions were performed simultaneously in the range between 1 and 15 min. The XRD patterns of the washed powders after this combined approach are present in Figure 3. The XRD patterns prior to washing procedure containing a large number of various reflections hard to identify are provided in the ESI (Figure S3).

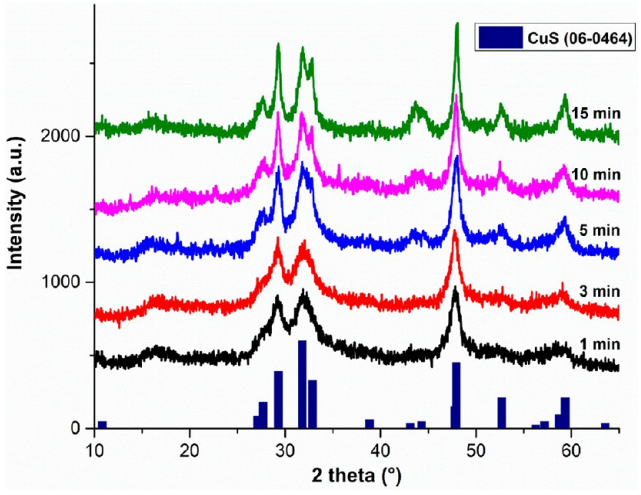

Figure 3. XRD patterns of mechanochemically synthesized copper sulfide prepared by a combined approach for a different milling time (nCuS).

DOI: 10.1021/acssuschemeng.9b01849
ACS Sustainable Chem. Eng. 2019, 7, 12897−12909

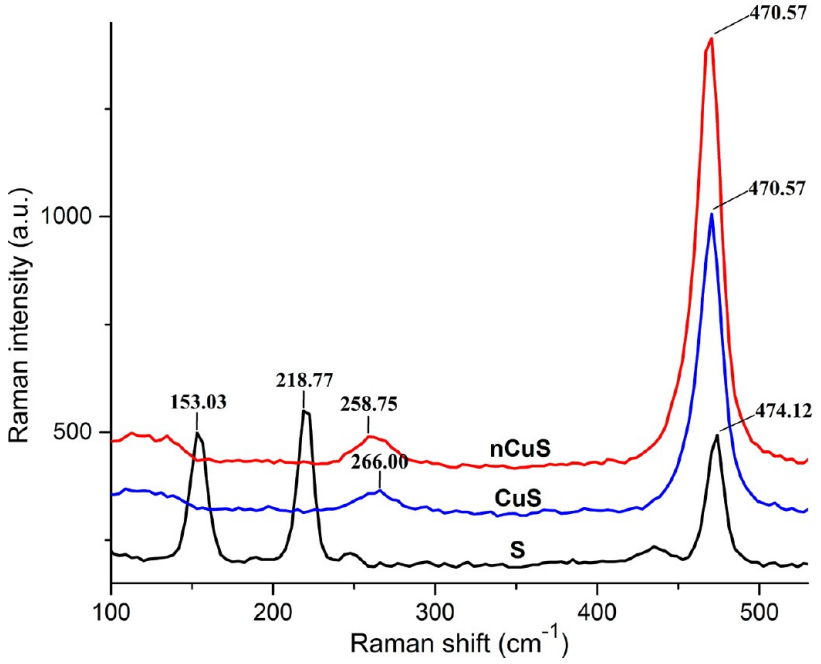

Figure 4. Raman spectra of S, CuS, and nCuS samples.

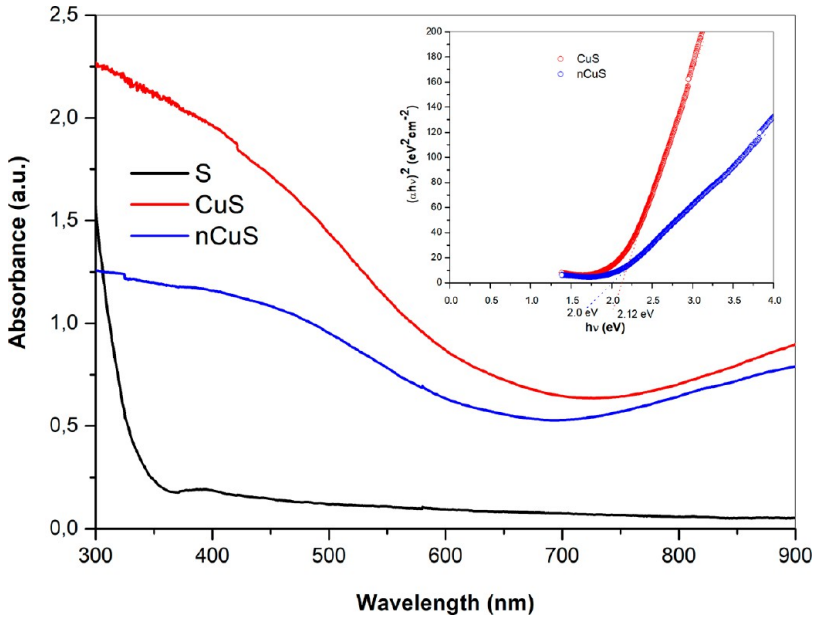

Figure 5. UV−vis absorption spectra of S, CuS, and nCuS samples (Tauc's plots with the determined energy band gaps are presented in the inset).

Standard copper sulfide peaks (JCPDS 06-0464) distinctly confirm the presence of copper sulfide particles in all the washed samples. The size of nanocrystals seems to be larger than when solely acetate route was used (Figure 2), as the peaks are sharper and more intensive. Sulfur was not identified in neither of the XRD patterns. The reason for this could be its quick amorphization during the milling process,[53] or the fact that it in situ undergoes further reaction. As the iron contamination was not detected in this case (on the contrary to synthesis of S), it is probable that the phenomena taking place during this combined approach are different from the situation when each step is performed individually. This point will be discussed later.

Raman Spectroscopy Analysis. Raman spectroscopy was used to characterize the three samples prepared by mechanochemical synthesis for 5 min (sulfur (S), and copper sulfide prepared either by acetate route (CuS) or by a combined approach (nCuS)). These samples were selected as final products and therefore, further characterization was peformed only on them.

As can be seen in Figure 4, three strong peaks were evidenced for S sample. According to refs 54 and 55, the main sulfur peaks should be located at 152, 220, and 474 cm^{-1}. In our case, the bands at 153.03, 218.77, and 474.12 cm^{-1} were found, which definitely confirm its presence.

The Raman spectrum of copper sulfide prepared by acetate route (CuS) contains two distinguishable peaks at 266.00 and 470.57 cm^{-1}. According to literature data, the main wavenumbers defining peaks of copper sulfide are located at 265 and

DOI: 10.1021/acssuschemeng.9b01849
ACS Sustainable Chem. Eng. 2019, 7, 12897−12909

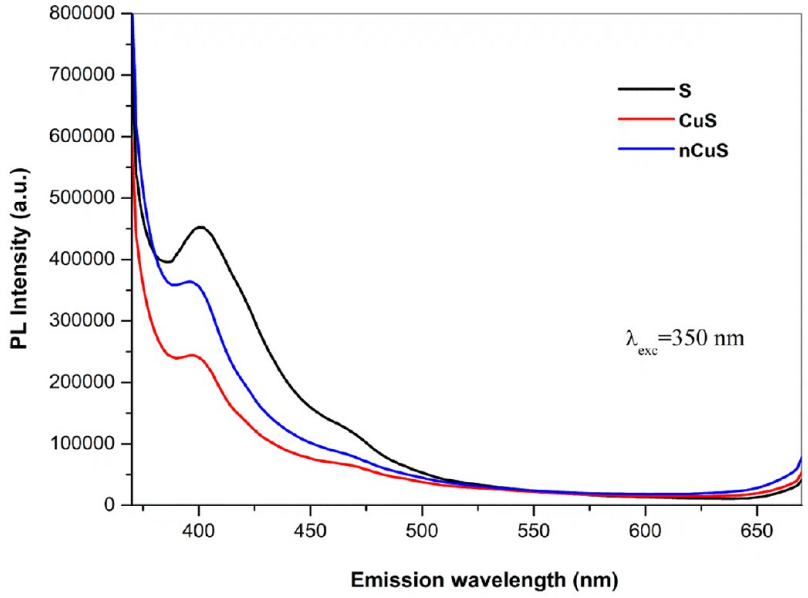

Figure 6. PL emission spectra of S, CuS, and nCuS samples at an excitation wavelength of 350 nm.

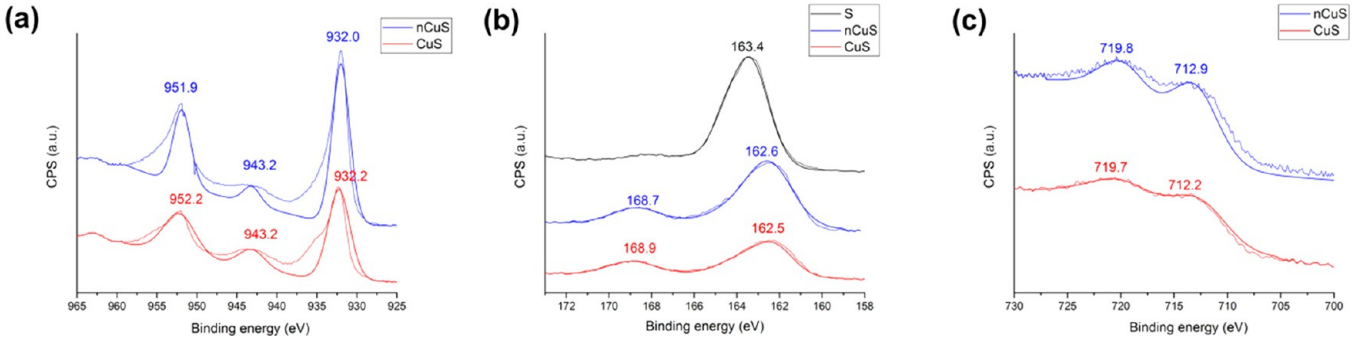

Figure 7. XPS spectra of S, CuS, and nCuS samples: (a) Cu 2p, (b) S 2p, and (c) Fe 2p. Bold lines show the results of fitting and the thin lines the experimental data.

473.5 cm^{-1},[56−58] so our results match with these values providing another proof of successful CuS synthesis.

In the nCuS sample, sulfur signals are absent, similarly to the XRD results of this sample. We could observe only copper sulfide peaks at wavenumbers 258.75 and 470.57 cm^{-1}. Although the absence of sulfur peaks in the nCuS sample can be explained by too small size of sulfur crystals, which makes it difficult to measure with Raman spectroscopy due to the phonon confinement effect,[59] its absence could also mean its transformation into some water-soluble compound and its washing out during the post-treatment of the milled mixture with distilled water (this will be discussed later).

UV−vis Spectroscopy Analysis. Figure 5 shows the differences in the visible range of UV−Vis absorption spectra of S, CuS and nCuS samples with clearly higher intensity of light absorbance for CuS-containing samples. The optical band gap, Eg was estimated based on Tauc equation for directly allowed optical transition $\alpha h\nu = A(h\nu - Eg)^{1/2}$ by the plotting $(\alpha h\nu)^2$ against photon energy and extrapolating the slope in the band edge region to zero, as shown in the inset of Figure 5. The optical band gap was determined to be 2.12 eV for CuS and 2.0 eV for nCuS. In the wavelength of the optical spectra, a blue shift was not found in comparison with the bulk CuS which has characteristic band gap energy of about 2.2 eV.[60] The determined band gaps are in accordance with the results published in previous papers.[61−63]

PL Spectroscopy. The room temperature PL spectra of S, CuS, and nCuS samples were obtained using excitation wavelength 350 nm and are displayed in Figure 6. CuS and nCuS samples exhibit a very weak emission at about 398 and 397 nm (corresponding to 3.096 and 3.104 eV) almost consistent with the literature.[64] Our results are different from previous papers, where no emission was reported[65] but, on the other hand, are in accordance with results reported in our earlier papers.[66,67] The observed photoluminescence intensity of nCuS sample is higher than in the case of CuS. The PL spectrum of S shows an emission peak at 400 nm (3.08 eV) and a small shoulder peak at 470 nm (corresponding to 2.63 eV) (Figure 5. The peak intensity is influenced by several parameters such as shapes, crystallinities, size effects of the products, which, in turn account for the increase in the content of surface oxygen vacancy and defects with a decrease in dimension.[68]

It can be seen that the synthesized S, CuS and nCuS samples have a little bit different optical properties. The band gap energy depends on the crystalline structure, size as well as morphology of the CuS nanostructures.

XPS Analysis. In order to investigate the oxidation states of the most abundant elements, the XPS spectra were recorded (Figure 7).

DOI: 10.1021/acssuschemeng.9b01849
ACS Sustainable Chem. Eng. 2019, 7, 12897−12909

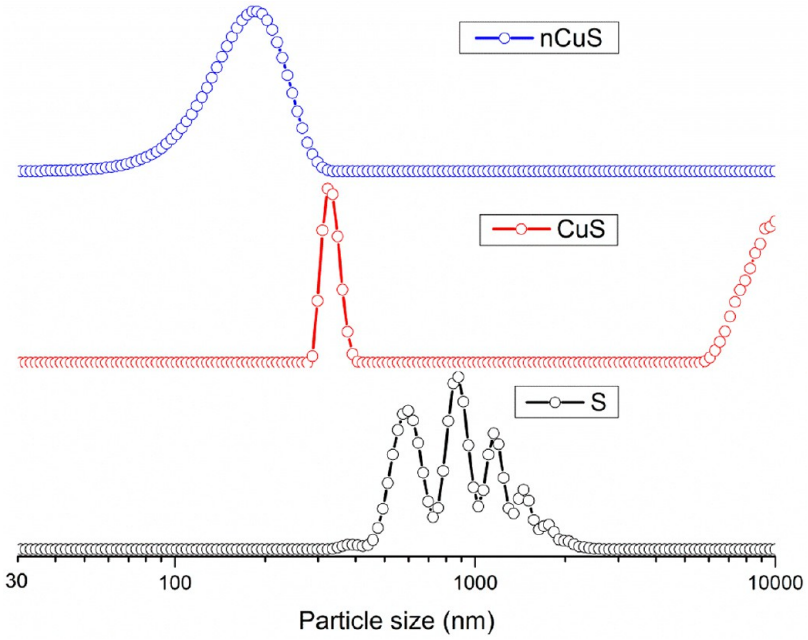

Figure 8. Particle size distribution of S, CuS, and nCuS samples.

The results showed the anticipated results in terms of oxidation states of all elements. In the case of copper (Figure 7a), the spectra are practically identical, showing the Cu in oxidation state +II (peaks around 952 and 932 eV). The satellite peak at 943.2 eV further confirms this.[66,69,70] There is a dispute about the presence of Cu in oxidation state +I cannot be overlooked.[71] In the case of sulfur (Figure 7b), the presence of S(-II) is clear (the peak around 162.5 eV).[66,69,70] However, also some oxidized species are present on the surface, as the peak around 168.8 corresponding to S(+VI) was found for both samples.[72] Sulfur sample exhibits the peak at 163 eV, which is in accordance for the binding energy reported for elemental sulfur in other studies.[73,74] Regarding iron coming from milling media, it was registered only in the case of CuS and nCuS samples. Its content seems to be higher in the case of nCuS. The results are different from XRD, where Fe was detected for pure sulfur, but it was not detected in the CuS sample (Figures 1 and 2). However, XPS is a surface method, so the distribution of elements can be different in comparison with the bulk analyzed by XRD. Iron was definitely oxidized into ionic form. It cannot be surely claimed whether it is in (+II) or (+III) state, as the XPS peaks are quite close and the binding energy depends also on the anion in the compound.[75] Nevertheless, its interaction with the milled powder and incorporation into some compound, mostly in the form of sulfate is in accordance with the results of XRD of the dried filtrate which will be reported later (Figure 13) and with the presence of sulfate peak in the S 2p spectrum (Figure 7b).

PCCS Analysis. Particle size distributions of the prepared samples are shown in Figure 8. Sulfur particles (S sample) are characterized by the polymodal distribution composed of several more-or-less discrete fractions. The sizes of particles are of a wide range (from 330 to 2600 nm). In the case of CuS nanoparticles synthesized by acetate route (CuS), the polymodal distribution was obtained in the measured range. The sample consists of particles with very fine sizes (from 280 to 410 nm) as well as of the coarse (or agglomerated) ones with the sizes of several micrometers. The unimodal particle size distribution was obtained for the sample prepared by a combined approach (nCuS). The fraction is very fine (from 40 to 330 nm) with the average hydrodynamic diameter of 170 nm.

Microstructural and Morphological Analyses. Figure 9 shows the results of the SEM analysis of mechanochemically synthesized S, CuS, and nCuS samples. SEM images of the sulfur sample (Figure 9a,b) showed that the sulfur particles are slightly larger than the other ones, thereby confirming the results of the PCCS analysis. The SEM-EDS results (see Figure 10a, S sample) also confirmed the results of XRD analysis showing the presence of iron and chromium in the sample. Also nickel and silicon are present in small amounts in the sample. Silicon can be present as a result of the cleaning procedure applied before the experiment, in which grinding balls and steel chamber are cleaned using abrasive sand with SiO_2 as the main component. The presence of Cr and Ni could be due to wear coming from steel milling chamber, as this element can be introduced into steel when it is produced.

In the case of both CuS samples, it is evident that the individual nanoparticles are agglomerated into large grains. SEM images of CuS produced by acetate route (Figure 9c,d) show that the copper sulfide particles have nonuniform sizes. It was already shown by PCCS analysis of this sample that it exhibits the polymodal distribution of particles (Figure 8). On the contrary to the produced sulfur, the EDS results did not show any impurities indicating high purity of the sample.

The SEM results of nCuS produced by sulfur-mediated acetate route synthesis (Figure 9e,f), it can be seen that the particles exhibit significantly different morphology from CuS sample produced by simple acetate route. More light on the shape of particles will be shed in the next paragraph (TEM analysis). The EDS results revealed the presence of wear and impurity in this sample, documented by Si, Fe, and Cr peaks in the spectra. However, the intensity of the corresponding peaks is smaller compared to the sulfur sample, so the wear is not so significant in the case, as it was not detected by XRD (Figure 3).

In order to reveal the morphology of CuS nanoparticles in the products, TEM analysis was performed. The sulfur particles

DOI: 10.1021/acssuschemeng.9b01849
ACS Sustainable Chem. Eng. 2019, 7, 12897−12909

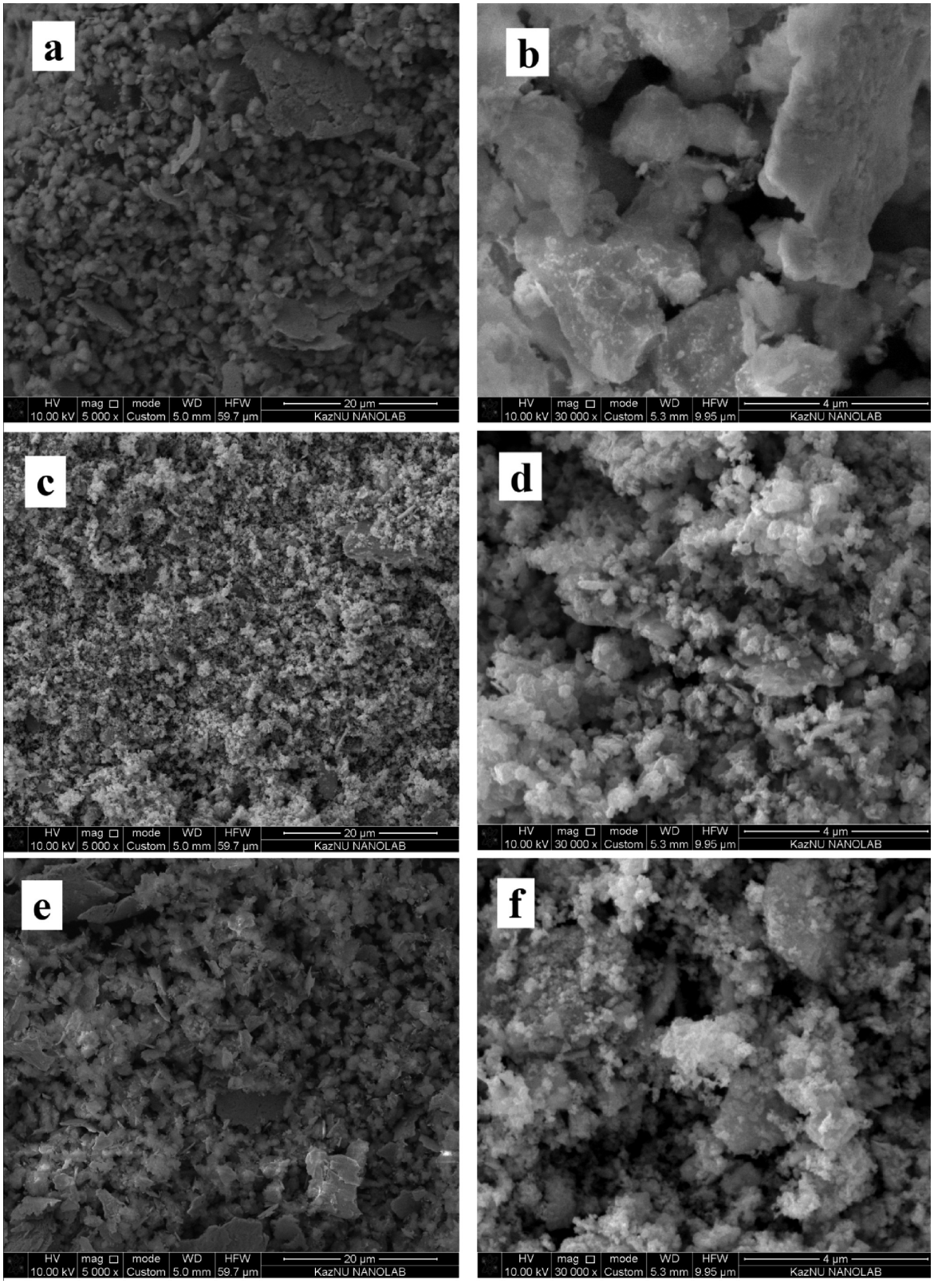

Figure 9. SEM images of mechanochemically synthesized sulfur (a, b), CuS (c, d), and nCuS (e, f) samples.

underwent detrimental changes under the high-energy electron beam, therefore, only CuS and nCuS samples were analyzed. Low-magnification images (Figure 11a,b) confirmed the observations by SEM that both samples are composed of agglomerated nanoparticles. Selected-area electron diffraction (SAED) patterns were recorded and only reflections from covellite (CuS) phase were found in both samples. The difference in the morphology of nanoparticles between the samples was revealed at higher magnifications. HRTEM images (Figure 11c,d) show that in the CuS sample, the crystallites are

DOI: 10.1021/acssuschemeng.9b01849
ACS Sustainable Chem. Eng. 2019, 7, 12897−12909

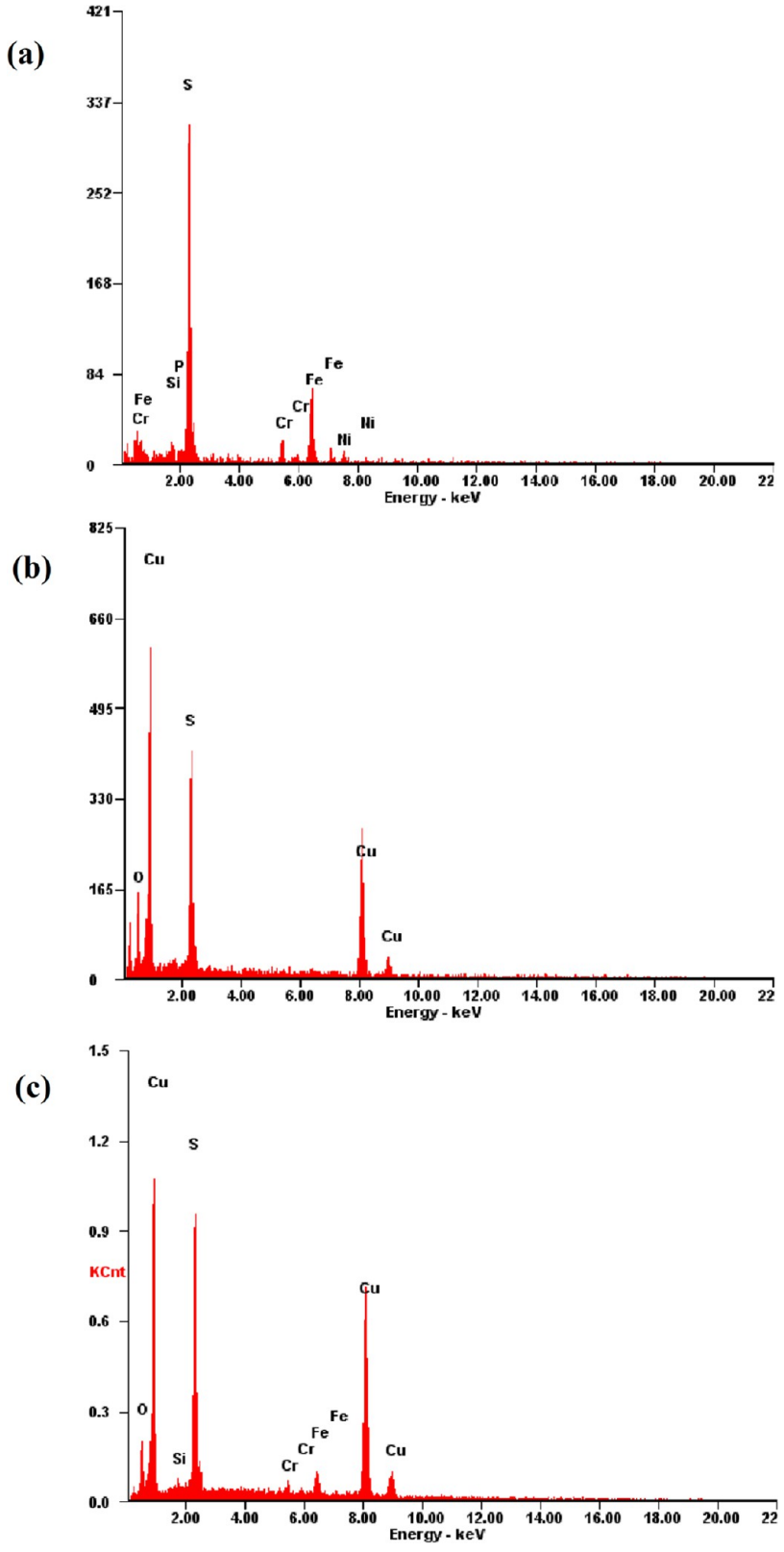

Figure 10. EDS results of mechanochemically synthesized S (a), CuS (b), and nCuS (c) samples.

tightly packed; they have more or less isometric morphology and size (diameter) in the range of 20 nm. The morphology of individual CuS crystallites is different in the nCuS sample. Here, most of the crystallites show elongated or needle-like shape with a thickness in the range between 6 and 8 nm and lengths up to 60 nm (aspect ratio up to 1:10). HRTEM analysis of the crystallites revealed that the particles are elongated along the basal planes of the covellite structure.

The difference in morphology of CuS NPs in both samples implies differences in the nucleation and growth mechanism of

DOI: 10.1021/acssuschemeng.9b01849
ACS Sustainable Chem. Eng. 2019, 7, 12897−12909

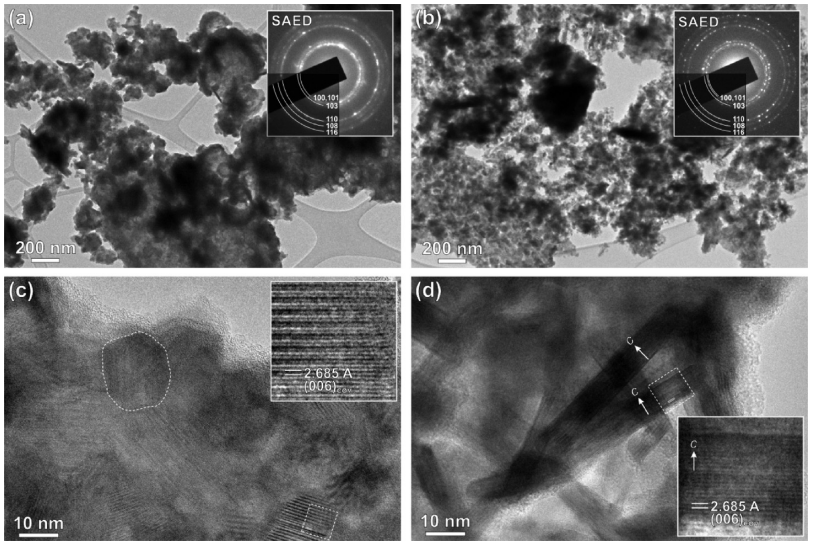

Figure 11. Low-magnification images with SAED patterns in the insets of (a) CuS and (b) nCuS samples confirm that both samples are composed of agglomerated nanoparticles. All rings in the SAED pattern belong to covellite (JCPDS 06-0464), (*hkl*) of lattice planes for the most intense rings are given. (c, d) High-resolution TEM images of both samples reveal the difference in the morphology of nanoparticles in both samples. (c) In the CuS sample, the NPs are nearly isometric, while in the (d) nCuS sample, the particles are elongated along basal (00l) planes (perpendicular to the *c*-axis, denoted by arrows) of the CuS covellite structure.

CuS under different synthesis conditions. The reasons may lie in the unique properties of the covellite structure (Figure 12a),

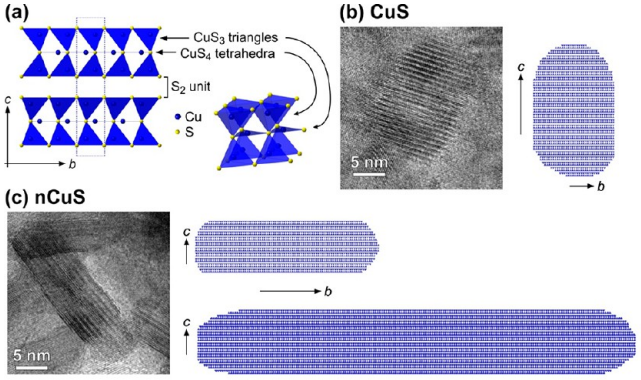

Figure 12. (a) Crystal structure of CuS. (b) Nearly isometric CuS NPs in the sample obtained by acetate route. (c) Elongated, needle-like CuS NPs with an aspect ratio up to 1:10 are observed in the sample synthesized in the presence of elemental sulfur.

which is composed of main structural units including Cu atoms in tetrahedral and triangular planar coordination and S−S bonds between these main units.[76] In the CuS sample prepared via the acetate route, the reaction between the precursors results in relatively uniform growth rates in all directions or a slightly faster growth rate in the *c*-direction (Figure 12b). On the other hand, the presence of elemental sulfur shows a significant effect on the crystal growth of CuS NPs. The nanoparticles have needle-like shape with a uniform thickness of around 6 nm length of up to 60 nm (aspect ratio 1:10) as shown in Figure 12c. The presence of elemental sulfur may enhance the S−S bonding and preferential growth of CuS along the basal planes (Figure 12c). This could be potentially interesting for particular applications since CuS exhibits superconducting-like behavior at temperatures below 40 K due to the structural characteristics.[76]

As elemental sulfur was not detected in the nCuS produced by a combined approach, it is highly probable that it reacted *in situ* to form a water-soluble compound.

From our point of view, the following reaction can occur:

$$2Cu(CH_3COO)_2\cdot H_2O + Na_2S_2O_3\cdot 5H_2O + C_6H_8O_7 + Na_2S\cdot 9H_2O + 8O_2 \rightarrow 2CuS + Na_2SO_4 + Na_2CO_3 + 22H_2O + 7CO_2 + C_6H_8O_7 \quad (4)$$

According to this reaction, there are three sulfur atoms entering the reaction. Two of them end in CuS product. The first one comes from the acidic decomposition sodium thiosulfate (reaction 1). We are of the opinion that it is present also in elemental form for a short time, thus serving as a nucleation agent. The second one comes from sodium sulfide. The last one is oxidized from sodium sulfite (product of reaction 1) into sodium sulfate. In order to prove this hypothesis, we recorded the XRD pattern of the dried filtrate (Figure 13). A small amount of CuS (JCPDS 06-0464) was identified. In addition to this, also Na_2SO_4 (JCPDS 79-1553) and $Na_2CO_3\cdot 10H_2O$ (JCPDS 01-0938) were found, thus supporting the idea about reaction 4). Possibly, also CuC_4O_4 (JCPDS 76-4595) and $Fe_4(OH)_{10}SO_4$ (JCPDS 21-0419) could be present. The presence of $Fe_4(OH)_{10}SO_4$ could be a result of the reaction between iron coming from milling media and side-products of reaction 4) in acidic conditions (due to the presence of citric acid). CuC_4O_4 can be hypothetically formed as a result of the reaction between Cu(+II) cations and acetate anions. For further information, the XRD patterns of the dried filtrates after 1 and 3 min are provided in ESI (Figure S4). The identified phases are more-or-less in accordance for the ones detected for the dried filtrate after nCuS synthesis for 5 min.

SEM, EDS, and Elemental Mapping Analysis. In order to examine the chemical changes going on during the nCuS formation (namely the absence of elemental sulfur in the final nCuS sample), the tools of SEM, EDS, and elemental mapping

DOI: 10.1021/acssuschemeng.9b01849
ACS Sustainable Chem. Eng. 2019, 7, 12897−12909

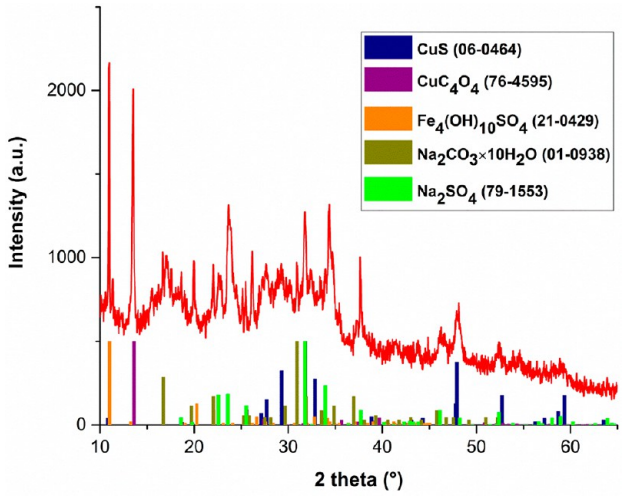

Figure 13. XRD pattern of dried filtrate of mechanochemically synthesized copper sulfide sample prepared by a combined approach for 5 min (nCuS).

were utilized. Namely, the not washed sample taken directly from the milling chamber and the dried filtrate obtained after the washing procedure of this sample were compared. The SEM images of both samples are provided in the ESI (Figures S5 and S6). Although the morphology is of secondary importance in this case, some phenomena can be observed. The not washed sample contains large particles of hundreds of microns with quite smooth morphology (Figure S5). The dried filtrate seems to be more structured with particles from a few microns up to 100 μm (Figure S6). The cracks observed in the image are most probably present due to the manual crashing of the obtained sample prior to analysis.

The chemical composition of both samples was investigated by means of EDS analysis. The results are summarized in Table 1.

Table 1. Results of the EDS Analysis of Not Washed Powder and Dried Filtrate from nCuS Synthesis (Values Are in at. %)

sample	region	Na	S	O	Cu	Fe
not washed	1	21.9	13.2	60.3	4.5	0.2
	2	22.4	11.8	61.5	4.2	0.2
	average	22.2	12.5	60.9	4.4	0.2
dried filtrate	1	24.1	14.1	60.2	1.5	0.2
	2	23.2	12.9	60.0	3.6	0.2
	3	26.2	10.0	61.8	1.6	0.5
	average	24.5	14.1	60.2	2.2	0.3

The difference between the two samples is not large. Both of them contain a significant amount of sodium, sulfur, and oxygen. The atomic ratio of these elements is quite close to the theoretical stoichiometry of sodium sulfate Na_2SO_4 (namely 28.6% of Na, 14.3% of S and 57.1% of O). This compound was identified in the XRD pattern of the dried filtrate (Figure 13), so sulfur formed in situ by eq 1) is most probably transformed into sodium sulfate upon further processing, according to eq 4. The only significant difference is in the copper content, which was two times higher for the not washed sample. As copper sulfide remained in the solid state during the washing process, the significant decrease of Cu content in the dried filtrate is logical. However, the content of sulfur was slightly lower for the not washed sample, which is contradictory and we are unable to explain this phenomenon at the moment. Iron content was on the borderline of the detection limit, so the contamination from milling media was not very significant in the analyzed regions.

The results of the elemental mapping of the dried filtrate after nCuS synthesis are shown in the Figure S7. Distribution of Na, S, and O is completely matching, which points to the fact that they are present in the same compound. This further supports the presence of Na_2SO_4. Copper seems to be concentrated in the area close to the middle of the image. The sulfur distribution in this region is also slightly richer, which points to the presence of a small amount of CuS (which was not effectively separated from the liquid phase during filtration). Its presence was also mentioned in the XRD pattern of the dried filtrate (see Figure 13). Iron seems to be evenly distributed, with some larger particles on the right side of the map. These particles can be fragments either from milling balls of the chamber.

Results of Antibacterial Activity Measurements. Three final samples (S, CuS and nCuS) in concentration 10 mg/mL were subjected to tests of antibacterial activity using agar well plate method on one Gram-negative (*E. coli*) and one Gram-positive (*S. aureus*) bacteria. The results are summarized in Figure 14.

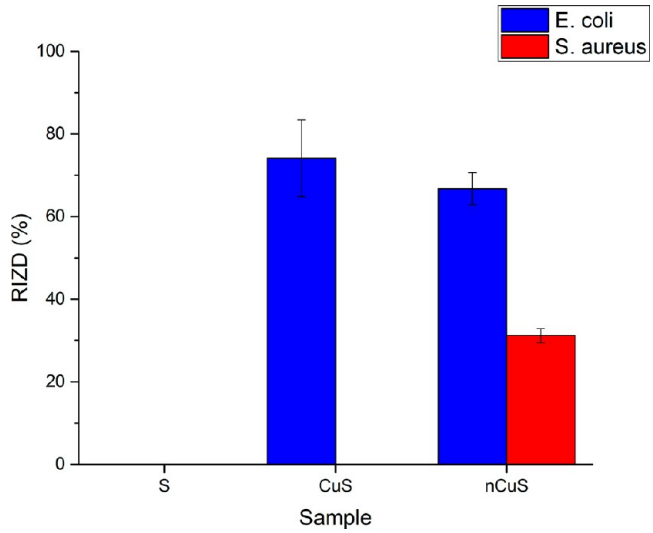

Figure 14. Antibacterial activity of S, CuS, and nCuS samples expressed as relative inhibition zones diameter (RIZD).

It can be seen that three studied samples exhibit significantly different antibacterial activity. The sulfur sample did not show any activity. However, the produced particles in our case are microsized and the antibacterial activity was reported to significantly increase upon the reduction of particle size into the nanorange.[77] The crystal structure, size and capping agent of sulfur NPs can have a significant effect on the antibacterial activity of sulfur.[77,78]

Copper sulfide prepared by acetate route has shown very strong antibacterial activity against Gram-negative *E. coli*, however, no activity for the Gram-positive *S. aureus* was evidenced. Although the formation of the even larger zones than for *E. coli* was evidenced in this case, the zones were not transparent and the borders were not strict so it was concluded that it is just some kind of reaction between the sample and the bacterial colonies, but it cannot be interpreted as antibacterial activity. On the contrary to the specificity of CuS sample, the

DOI: 10.1021/acssuschemeng.9b01849
ACS Sustainable Chem. Eng. 2019, 7, 12897−12909

nCuS one has shown the effect against both *E. coli* and *S. aureus*. Although the effect was approximately two times lower against *S. aureus*, the sulfur-mediated synthesis brought about an improvement of antibacterial activity in terms of being less selective. This creates a space for the investigation of the effect of CuS nanoparticles of various shapes on the antibacterial activity in the future.

It seems that the interaction between the CuS NPs and bacteria is quite specific. Such evidence was also reported in the first report on the antibacterial activity of CuS nanoparticles published in 2015,[18] in which no activity against *S. aureus* was found. The mechanism of action was found to be through damage of the cell wall. The authors also investigated the effect of copper(II) ions, which was found to be lower than the one of CuS NPs. Chakraborty et al.[79] suggest that the antibacterial effect of CuS is through disturbing the respiration process of the cell. This study is also interesting because it reports on the effect of different shape on the activity. Namely against *E. coli*, only granular particles exhibited activity, whereas the spherical and agglomerated ones did not. Another work investigated also the minimal inhibitory concentration of the spherical CuS NPs.[19] It was found to be 30 and 40 μg/mL for *E. coli* and *S. aureus*, respectively. The activities against both bacteria were more-or-less similar in this study. The zebrafish animal model was applied to study the antibacterial activity of CuS NPs in ref 20. The authors confirmed the main role of CuS NPs is in the membrane damage and triggering the production of reactive oxygen species. They also found that CuS NPs are hemocompatible. Finally, sheet-like CuS NPs were used as a coating for polyacrylonitrile fibers and the material showed the antibacterial efficacy 99.99% against *S. aureus* and 96.80% against *E. coli*.[80]

CONCLUSION

A rapid environmentally friendly mechanochemical synthesis of copper sulfide nanocrystals yielding different shapes is proposed for the first time in this report. The synthesis is completed in just 5 min. TEM analysis showed that the utilization of sulfur as a nucleation agent can lead to the formation of needle-like CuS (nCuS) nanocrystals with an elongated shape. This phenomenon did not occur when CuS was produced by simple cogrinding of precursors, as the nanocrystals exhibited a spherical shape in this case. Results of photon cross-correlation spectroscopy showed that the size of agglomerates is significantly smaller for nCuS sample. The produced CuS nanoparticles exhibit antibacterial activity. It was found that nCuS is a less selective agent, as it possessed activity against both *E. coli* and *S. aureus* bacteria, whereas the spherical CuS sample showed activity only against *E. coli*. The present study could possibly serve as a protocol for the shape-controlled synthesis of nanoparticles using mechanochemistry, which could open a new branch of this environmentally friendly and sustainable synthetic method.

ASSOCIATED CONTENT

Supporting Information

The Supporting Information is available free of charge on the ACS Publications website at DOI: 10.1021/acssuschemeng.9b01849.

XRD patterns of the not washed samples treated for different time, XRD pattern of the dried filtrates of the nCuS sample treated for 1 and 3 min, SEM images of nCuS sample treated for 5 min prior to washing and corresponding dried filtrate after washing, and elemental mapping results of this dried filtrate (PDF)

AUTHOR INFORMATION

Corresponding Author

*E-mail: zhandos.shalabay@gmail.com.

ORCID

Zh. Shalabayev: 0000-0003-3465-8241

M. Baláž: 0000-0001-6563-7588

Notes

The authors declare no competing financial interest.

ACKNOWLEDGMENTS

This work was supported by the Ministry of Education and Science of Kazakhstan Republic (Grant Nos. BR05234566 and AP05133115). It was also financially supported by the Slovak Research and Development Agency under Contract No. APVV-18-0357 and by the Slovak Grant Agency VEGA (Project 2/0044/18). N.D. acknowledges financial support from the Slovenian Research Agency (research core funding No. P2-0091). The support of Ministry of Science and Higher Education of the Russian Federation (RFBR grants 18-05-00434A and 19-45-540003p_a) is also gratefully acknowledged.

REFERENCES

(1) Baláž, P.; Baláž, M.; Achimovičová, M.; Bujňáková, Z.; Dutková, E. Chalcogenide mechanochemistry in materials science: insight into synthesis and applications (a review). *J. Mater. Sci.* **2017**, *52*, 11851−11890.

(2) Ryan, K. M.; Cabot, A.; Coughlan, C.; Ibáñez, M.; Dobrozhan, O.; Singh, A. Compound copper chalcogenide nanocrystals. *Chem. Rev.* **2017**, *117* (9), 5865−6109.

(3) Plass, K. E.; Rossi, D. P.; Machani, T.; Lotfipour, M. α-chalcocite nanoparticle synthesis and stability. *Chem. Mater.* **2011**, *23* (12), 3032−3038.

(4) Bera, P.; Mondal, G.; Bera, P.; Santra, A.; Jana, S.; Mandal, T. N.; Mondal, A.; Seok, S. I. Precursor-driven selective synthesis of hexagonal chalcocite (Cu_2S) nanocrystals: structural, optical, electrical and photocatalytic properties. *New J. Chem.* **2014**, *38* (10), 4774−4782.

(5) Saranya, M.; Santhosh, C.; Ramachandran, R.; Kollu, P.; Saravanan, P.; Vinoba, M.; Jeong, S. K.; Grace, A. N. Hydrothermal growth of CuS nanostructures and its photocatalytic properties. *Powder Technol.* **2014**, *252*, 25−32.

(6) Shamraiz, U.; Hussain, R. A.; Badshah, A. Fabrication and applications of copper sulfide (CuS) nanostructures. *J. Solid State Chem.* **2016**, *238*, 25−40.

(7) Wang, K.; Tan, G. L. Synthesis and optical properties of CuS nanocrystals by mechanical alloying process. *Curr. Nanosci.* **2010**, *6* (2), 163−168.

(8) Roy, P.; Srivastava, S. K. Nanostructured copper sulfides: synthesis, properties and applications. *CrystEngComm* **2015**, *17* (41), 7801−7815.

(9) Xie, Y.; Jiang, X.; Lu, J.; He, W.; Zhu, L.; Qiana, Y. Preparation and phase transformation of nanocrystalline copper sulfides (Cu_9S_8, Cu_7S_4 and CuS) at low temperature. *J. Mater. Chem.* **2000**, *10* (9), 2193−2196.

(10) Zhang, Y.; Qiao, Z.-P.; Chen, X.-M. Microwave-assisted elemental-direct-reaction route to nanocrystalline copper sulfides Cu_9S_8 and Cu_7S_4. *J. Solid State Chem.* **2002**, *167* (1), 249−253.

(11) Chen, W. Tianyue Qian, Hongliang Cao, Shoushuang Huang, Qingquan He, Na Liang, Cheng Wang, Jiantao Zai, Rational design and fabrication of skeletal Cu_7S_4 nanocages for efficient counter electrode in quantum dot-sensitized solar cells. *Nano Energy* **2015**, *12*, 186−196.

DOI: 10.1021/acssuschemeng.9b01849
ACS Sustainable Chem. Eng. 2019, 7, 12897−12909

(12) Goel, S.; Chen, F.; Cai, W. B. Synthesis and biomedical applications of copper sulfide nanoparticles: From sensors to theranostics. *Small* **2014**, *10* (4), 631−645.
(13) Suh, M. P.; Cho, K.; Han, S.-H. Copper-organic framework fabricated with CuS nanoparticles: synthesis, electrical conductivity, and electrocatalytic activities for oxygen reduction reaction. *Angew. Chem., Int. Ed.* **2016**, *55* (49), 15301−15305.
(14) Grozdanov, I.; Najdoski, M. Optical and electrical properties of copper sulfide films of variable composition. *J. Solid State Chem.* **1995**, *114* (2), 469−475.
(15) Nair, P. K.; Nair, M. T. S.; Pathirana, H. M. K. K.; Zingaro, R. A.; Meyers, E. A. Structure and composition of chemically deposited thin films of bismuth sulfide and copper sulfide - effect on optical and electrical properties. *J. Electrochem. Soc.* **1993**, *140* (3), 754−759.
(16) Fan Zhang, H.-Q. Z. Wenming Zhang, Jun Yin, Fu-Hu Cao, Yun-Xiang Pan, Noble-metal-free CuS/CdS photocatalyst for efficient visible-light-driven photocatalytic H_2 production from water. *Catal. Today.* **2019**, *330*, 203−208.
(17) Chattopadhyay, T.; Chakraborty, P.; Adhikary, J.; Chatterjee, S.; Biswas, B. Facile syntheses of copper sulfide nanoparticles: antibacterial and antifungal activity study. *Rasayan Journal of Chemistry* **2016**, *9* (1), 77−83.
(18) Wang, H.-Y.; Hua, X.-W.; Wu, F.-G.; Li, B.; Liu, P.; Gu, N.; Wang, Z.; Chen, Z. Synthesis of ultrastable copper sulfide nanoclusters via trapping the reaction intermediate: potential anticancer and antibacterial applications. *ACS Appl. Mater. Interfaces* **2015**, *7* (13), 7082−7092.
(19) Malarkodi, C.; Rajeshkumar, S. In vitro bactericidal activity of biosynthesized CuS nanoparticles against UTI-causing pathogens. *Inorganic and Nano-Metal Chemistry* **2017**, *47* (9), 1290−1297.
(20) Ahmed, K. B. A.; Anbazhagan, V. Synthesis of copper sulfide nanoparticles and evaluation of in vitro antibacterial activity and in vivo therapeutic effect in bacteria-infected zebrafish. *RSC Adv.* **2017**, *7* (58), 36644−36652.
(21) Ingle, A. P.; Duran, N.; Rai, M. Bioactivity, mechanism of action, and cytotoxicity of copper-based nanoparticles: A review. *Appl. Microbiol. Biotechnol.* **2014**, *98* (3), 1001−1009.
(22) Hans, M.; Erbe, A.; Mathews, S.; Chen, Y.; Solioz, M.; Mucklich, F. Role of Copper Oxides in Contact Killing of Bacteria. *Langmuir* **2013**, *29* (52), 16160−16166.
(23) Chatterjee, A. K.; Chakraborty, R.; Basu, T. Mechanism of antibacterial activity of copper nanoparticles. *Nanotechnology* **2014**, *25*, 135101.
(24) Salavati-Niasari, M.; Alizadeh, S.; Mousavi-Kamazani, M.; Mir, N.; Rezaei, O.; Ahmadi, E. Surfactant-free fabrication of copper sulfides (CuS, Cu_2S) via hydrothermal method. *J. Cluster Sci.* **2013**, *24* (4), 1181−1191.
(25) Yan, H.; Yaping, W.; Wenhong, G.; Yijing, W.; Lifang, J.; Huatang, Y.; Shuangxi, L. Synthesis of novel CuS with hierarchical structures and its application in lithium-ion batteries. *Powder Technol.* **2011**, *212* (1), 64−68.
(26) Cheng, F. M.; Qi, Z. Y.; Xiao, F. Q.; Gen, T. Z.; Mao, L. L.; Sheng, Q. F. Controlled synthesis of various hierarchical nanostructures of copper sulfide by a facile microwave irradiation method. *Colloids and Surfaces A-physicochemical and Engineering Aspects* **2010**, *371* (1−3), 14−21.
(27) Guangzhao, M.; Wenfei, D.; Dirk, G. K.; Helmuth, M. Synthesis of copper sulfide nanorod arrays on molecular templates. *Nano Lett.* **2004**, *4* (2), 249−252.
(28) Guozhen, S.; Di, C.; Kaibin, T.; Xianming, L.; Liying, H.; Yitai, Q. General synthesis of metal sulfides nanocrystallines via a simple polyol route. *J. Solid State Chem.* **2003**, *173* (1), 232−235.
(29) Reijnen, L.; Meester, B.; Lange, F. D.; Schoonman, J.; Goossens, A. Comparison of Cu_xS films grown by atomic layer deposition and chemical vapor deposition. *Chem. Mater.* **2005**, *17* (10), 2724−2728.
(30) Baláž, M.; Zorkovská, A.; Urakaev, F.; Baláž, P.; Briančin, J.; Bujňáková, Z.; Achimovičová, M.; Gock, E. Ultrafast mechanochemical synthesis of copper sulfides. *RSC Adv.* **2016**, *6* (91), 87836−87842.
(31) Zhang, B.-P.; Li, S.; Ge, Z.-H.; Yao, Y.; Wang, H.-C.; Yanga, J.; Li, Y.; Gao, C.; Lin, Y.-H. Mechanochemically synthesized sub-5 nm sized CuS quantum dots with high visible-light-driven photocatalytic activity. *Appl. Surf. Sci.* **2016**, *384*, 272−278.
(32) Baláž, M.; Zorkovská, A.; Blazquez, J. S.; Daneu, N.; Baláž, P. Mechanochemistry of copper sulphides: Phase interchanges during milling. *J. Mater. Sci.* **2017**, *52* (20), 11947−11961.
(33) Tan, D.; Garcia, F. Main group mechanochemistry: from curiosity to established protocols. *Chem. Soc. Rev.* **2019**, *48* (8), 2274−2292.
(34) Baláž, P.; Achimovičová, M.; Baláž, M.; Billik, P.; Cherkezova-Zheleva, Z.; Criado, J. M.; Delogu, F.; Dutková, E.; Gaffet, E.; Gotor, F. J.; Kumar, R.; Mitov, I.; Rojac, T.; Senna, M.; Streletskii, A.; Wieczorek-Ciurowa, K. Hallmarks of mechanochemistry: from nanoparticles to technology. *Chem. Soc. Rev.* **2013**, *42* (18), 7571−7637.
(35) James, S. L.; Adams, C. J.; Bolm, C.; Braga, D.; Collier, P.; Friščić, T.; Grepioni, F.; Harris, K. D. M.; Hyett, G.; Jones, W.; Krebs, A.; Mack, J.; Maini, L.; Orpen, A. G.; Parkin, I. P.; Shearouse, W. C.; Steed, J. W.; Waddell, D. C. Mechanochemistry: opportunities for new and cleaner synthesis. *Chem. Soc. Rev.* **2012**, *41* (1), 413−447.
(36) Groote, R.; Jakobs, R. T. M.; Sijbesma, R. P. Mechanocatalysis: forcing latent catalysts into action. *Polym. Chem.* **2013**, *4* (18), 4846−4859.
(37) May, P. A.; Moore, J. S. Polymer mechanochemistry: techniques to generate molecular force via elongational flows. *Chem. Soc. Rev.* **2013**, *42* (18), 7497−7506.
(38) Braga, D.; Maini, L.; Grepioni, F. Mechanochemical preparation of co-crystals. *Chem. Soc. Rev.* **2013**, *42* (18), 7638−7648.
(39) Guo, X. Y.; Xiang, D.; Duan, G. H.; Mou, P. A review of mechanochemistry applications in waste management. *Waste Manage.* **2010**, *30* (1), 4−10.
(40) Boldyreva, E. Mechanochemistry of inorganic and organic systems: what is similar, what is different? *Chem. Soc. Rev.* **2013**, *42* (18), 7719−7738.
(41) Baláž, P.; Boldižárová, E.; Godočíková, E.; Briančin, J. Mechanochemical route for sulphide nanoparticles preparation. *Mater. Lett.* **2003**, *57* (9−10), 1585−1589.
(42) Godočíková, E.; Baláž, P.; Gock, E.; Choi, W. S.; Kim, B. S. Mechanochemical synthesis of the nanocrystalline semiconductors in an industrial mill. *Powder Technol.* **2006**, *164* (3), 147−152.
(43) Tang, K.; Chen, D.; Liu, Y.; Shen, G.; Zheng, H.; Qian, Y. Shape-controlled synthesis of copper sulfide nanocrystals via a soft solution route. *J. Cryst. Growth* **2004**, *263* (1−4), 232−236.
(44) Du, W.; Qian, X.; Ma, X.; Gong, Q.; Cao, H.; Yin, J. Shape-controlled synthesis and self-assembly of hexagonal covellite (CuS) nanoplatelets. *Chem. - Eur. J.* **2007**, *13* (11), 3241−3247.
(45) Cao, J.; Ji, H.; Feng, J.; Chang, X.; Ma, X.; Liu, J.; Zheng, M. Fabrication of CuS nanocrystals with various morphologies in the presence of a nonionic surfactant. *Mater. Lett.* **2005**, *59* (24−25), 3169−3172.
(46) Zhang, Y. C.; Hu, X. Y.; Qiao, T. Shape-controlled synthesis of CuS nanocrystallites via a facile hydrothermal route. *Solid State Commun.* **2004**, *132* (11), 779−782.
(47) Junhua Li, M. L. Morphology-controlled electrochemical sensing properties of CuS crystals for tartrazine and sunset yellow. *Sens. Actuators, B* **2019**, *288* (1), 552−563.
(48) Urakaev, F. K.; Bulavchenko, A. I.; Uralbekov, B. M.; Massalimov, I. A.; Tatykayev, B. B.; Bolatov, A. K.; Dzharlykasimova, D. N.; Burkitbayev, M. M. Mechanochemical synthesis of colloidal sulfur particles in the $Na_2S_2O_3$-H-2($C_4H_4O_4$)-Na_2SO_3 system. *Colloid J.* **2016**, *78* (2), 210−219.
(49) Rojas, J. J.; Ochoa, V. J.; Ocampo, S. A.; Muñoz, J. F. Screening for antimicrobial activity of ten medicinal plants used in Colombian folkloric medicine: A possible alternative in the treatment of non-nosocomial infections. *BMC Complementary Altern. Med.* **2006**, *6*, 2.
(50) Urakaev, F. K. Preparation of $NaIn(WO_4)_2$ nanocrystals and a charge for crystal growth via the free-of-rubbing mechanical activation of the Na_2CO_3-In_2O_3-WO_3 system. *Mendeleev Commun.* **2016**, *26* (6), 546−548.

DOI: 10.1021/acssuschemeng.9b01849
ACS Sustainable Chem. Eng. 2019, 7, 12897−12909

(51) Dodd, A. C.; McCormick, P. G. Synthesis of nanocrystalline ZrO_2 powders by mechanochemical reaction of $ZrCl_4$ with LiOH. *J. Eur. Ceram. Soc.* **2002**, *22* (11), 1823−1829.
(52) Tsuzuki, T.; Ding, J.; McCormick, P. G. Mechanochemical synthesis of ultrafine zinc sulfide particles. *Phys. B* **1997**, *239* (3−4), 378−387.
(53) Luo, H.; Ruoff, A. L. X-Ray-diffraction study of sulfur to 32 GPa - amorphization at 25 GPa. *Phys. Rev. B: Condens. Matter Mater. Phys.* **1993**, *48* (1), 569−572.
(54) Jaroudi, O. E.; Picquenard, E.; Gobeltz, N.; Demortier, A.; Corset, J. Raman spectroscopy study of the reaction between sodium sulfide or disulfide and sulfur: identity of the species formed in solid and liquid phases. *Inorg. Chem.* **1999**, *38* (12), 2917−2923.
(55) Wang, J.; Chenb, J.; Konstantinov, K.; Zhaoa, L.; Nga, S. H.; Wang, G. X.; Guoa, Z. P.; Liu, H. K. Sulphur-polypyrrole composite positive electrode materials for rechargeable lithium batteries. *Electrochim. Acta* **2006**, *51* (22), 4634−4638.
(56) Givalou, L.; Antoniadou, M.; Perganti, D.; Giannouri, M.; Karagianni, C. S.; Kontos, A. G.; Falarasa, P. Electrodeposited cobalt-copper sulfide counter electrodes for highly efficient quantum dot sensitized solar cells. *Electrochim. Acta* **2016**, *210*, 630−638.
(57) Tarachand; Hussainb, S.; Lallaa, N. P.; Kuoc, Y.-K.; Lakhania, A.; Sathea, V. G.; Deshpandea, U.; Okrama, G. S. Thermoelectric properties of Ag-doped CuS nanocomposites synthesized by a facile polyol method. *Phys. Chem. Chem. Phys.* **2018**, *20* (8), 5926−5935.
(58) Nemade, K. R.; Waghuley, S. A. Band gap engineering of CuS nanoparticles for artificial photosynthesis. *Mater. Sci. Semicond. Process.* **2015**, *39*, 781−785.
(59) Zuo, J.; Xu, C.; Liu, Y.; Qian, Y. Crystallite size effects on the Raman spectra of Mn_3O_4. *Nanostruct. Mater.* **1998**, *10* (8), 1331−1335.
(60) Haram, S. K.; Mahadeshwar, A. R.; Dixit, S. G. Synthesis and characterization of copper sulfide nanoparticles in Triton-X 100 water-in-oil microemulsions. *J. Phys. Chem.* **1996**, *100* (14), 5868−5873.
(61) Zhang, Y. Q.; Zhang, B. P.; Zhu, L. F. Monodisperse CuS nanodisks: low-temperature solvothermal synthesis and enhanced photocatalytic activity. *RSC Adv.* **2014**, *4* (103), 59185−59193.
(62) Huse, N. P.; Dive, A. S.; Gattu, K. P.; Sharma, R. An experimental and theoretical study on soft chemically grown CuS thin film for photosensor application. *Mater. Sci. Semicond. Process.* **2017**, *67*, 62−68.
(63) Tanveer, M.; Cao, C. B.; Ali, Z.; Aslam, I.; Idrees, F.; Khan, W. S.; But, F. K.; Tahir, M.; Mahmood, N. Template free synthesis of CuS nanosheet-based hierarchical microspheres: an efficient natural light driven photocatalyst. *CrystEngComm* **2014**, *16* (24), 5290−5300.
(64) Ou, S. M.; Xie, Q.; Ma, D. K.; Liang, J. B.; Hu, X. K.; Yu, W. C.; Qian, Y. T. A precursor decomposition route to polycrystalline CuS nanorods. *Mater. Chem. Phys.* **2005**, *94* (2−3), 460−466.
(65) Jiang, X. C.; Xie, Y.; Lu, J.; He, W.; Zhu, L. Y.; Qian, Y. T. Preparation and phase transformation of nanocrystalline copper sulfides (Cu_9S_8, Cu_7S_4 and CuS) at low temperature. *J. Mater. Chem.* **2000**, *10* (9), 2193−2196.
(66) Baláž, M.; Dutková, E.; Bujňáková, Z.; Tóthová, E.; Kostova, N. G.; Karakirova, Y.; Briančin, J.; Kaňuchová, M. Mechanochemistry of copper sulfides: Characterization, surface oxidation and photocatalytic activity. *J. Alloys Compd.* **2018**, *746*, 576−582.
(67) Achimovicova, M.; Dutkova, E.; Tothova, E.; Bujnakova, Z.; Briancin, J.; Kitazono, S. Structural and optical properties of nanostructured copper sulfide semiconductor synthesized in an industrial mill. *Front. Chem. Sci. Eng.* **2019**, *13* (1), 164−170.
(68) Jing, L. Q.; Qu, Y. C.; Wang, B. Q.; Li, S. D.; Jiang, B. J.; Yang, L. B.; Fu, W.; Fu, H. G.; Sun, J. Z. Review of photoluminescence performance of nano-sized semiconductor materials and its relationships with photocatalytic activity. *Sol. Energy Mater. Sol. Cells.* **2006**, *90* (12), 1773−1787.
(69) Ye, M. D.; Wen, X. R.; Zhang, N.; Guo, W. X.; Liu, X. Y.; Lin, C. J. In situ growth of CuS and $Cu_{1.8}S$ nanosheet arrays as efficient counter electrodes for quantum dot-sensitized solar cells. *J. Mater. Chem. A* **2015**, *3* (18), 9595−9600.
(70) Li, S.; Ge, Z. H.; Zhang, B. P.; Yao, Y.; Wang, H. C.; Yang, J.; Li, Y.; Gao, C.; Lin, Y. H. Mechanochemically synthesized sub-5 nm sized CuS quantum dots with high visible-light-driven photocatalytic activity. *Appl. Surf. Sci.* **2016**, *384*, 272−278.
(71) Nduna, M. K.; Lewis, A. E.; Nortier, P. A model for the zeta potential of copper sulphide. *Colloids Surf., A* **2014**, *441*, 643−652.
(72) Krylova, V.; Andrulevicius, M. Optical, XPS and XRD studies of semiconducting copper sulfide layers on a polyamide film. *Int. J. Photoenergy* **2009**, *2009*, 1.
(73) Hao, Q. Y.; Cui, G. L.; Tian, Y.; Tan, T. Z.; Zhang, Y. G. Three-dimensional S/CeO_2/RGO domposites as dathode daterials for lithium-sulfur batteries. *Materials* **2018**, *11* (9), 1720.
(74) Senkevich, J. J.; Yang, G. R.; Tang, F.; Wang, G. C.; Lu, T. M.; Cale, T. S.; Jezewski, C.; Lanford, W. A. Substrate-independent sulfur-activated dielectric and barrier-layer surfaces to promote the chemisorption of highly polarizable metallorganics. *Appl. Phys. A: Mater. Sci. Process.* **2004**, *79* (7), 1789−1796.
(75) Grosvenor, A. P.; Kobe, B. A.; Biesinger, M. C.; McIntyre, N. S. Investigation of multiplet splitting of Fe 2p XPS spectra and bonding in iron compounds. *Surf. Interface Anal.* **2004**, *36* (12), 1564−1574.
(76) Duarte, H. l. A.; Morales-García, A.; Antonio Lenito Soares, J.; Santos, E. C. D.; Abreu, H. A. d. First-principles calculations and electron density topological analysis of covellite (CuS). *J. Phys. Chem. A* **2014**, *118* (31), 5823−5831.
(77) Choudhury, S. R.; Mandal, A.; Ghosh, M.; Basu, S.; Chakravorty, D.; Goswami, A. Investigation of antimicrobial physiology of orthorhombic and monoclinic nanoallotropes of sulfur at the interface of transcriptome and metabolome. *Appl. Microbiol. Biotechnol.* **2013**, *97* (13), 5965−5978.
(78) Choudhury, S. R.; Roy, S.; Goswami, A.; Basu, S. Polyethylene glycol-stabilized sulphur nanoparticles: an effective antimicrobial agent against multidrug-resistant bacteria. *J. Antimicrob. Chemother.* **2012**, *67* (5), 1134−1137.
(79) Chakraborty, P.; Adhikari, J.; Chattarjee, S.; Biswas, B.; Chattopadhyay, T. Facile synthesis of copper sulfide nanoparticles: antibacterial and antifungal activity study. *Rasyan Journal of Chemistry* **2016**, *9*, 77−83.
(80) Wang, Y.; Wang, W.; Liu, B.; Yu, D. Preparation of durable antibacterial and electrically conductive polyacrylonitrile fibers by copper sulfide coating. *J. Appl. Polym. Sci.* **2017**, *134* (44), 45496.

DOI: 10.1021/acssuschemeng.9b01849
ACS Sustainable Chem. Eng. 2019, 7, 12897−12909